Journal of New Materials for Electrochemical Systems 15, 203-209 (2012)

Enhanced Capacitance of Microwave-assisted Functionalized Ordered Mesopourous Carbon for Supercapacitors

B. Portales-Martínez[1,*], R.G. González-Huerta[2], J.M. Domínguez-Esquivel[3] and C.A. Cortés-Escobedo[1]

[1]Centro de Investigación e Innovación Tecnológica del IPN, Cda. CECATI S/N Col. Sta. Catarina, Del. Azcapotzalco, México, D. F. CP 02250

[2]Escuela Superior de Ingeniería Química del IPN, Laboratorio de Electrocatálisis, Unidad Profesional Adolfo López Mateos, México, D. F. CP 07738

[3]Instituto Mexicano del Petróleo, Eje Central Lázaro Cárdenas Norte 152, Col. San Bartolo Atepehuacan, México, D. F. CP 07730

Received: November 27, 2011, Accepted: February 09, 2012, Available online: April 05, 2012

Abstract: *The electrochemical capacitance for a double layer of ordered mesoporous carbon (OMC) nanofibers functionalized under differing conditions is presented. OMC nanofibers were prepared using the molding method from SBA-15 and sucrose. Functionalisation was performed using varying HNO_3 concentrations at 110°C and 120°C assisted by microwave radiation over 3 minutes. The transmission electron micrographs of the resulting fibers are reported. The capacitance, surface area and functional groups as functions of the acidity and heat treatment were analysed via cyclic voltammetry, nitrogen adsorption-desorption, and X-ray photoelectron spectroscopy, respectively. Ordered nanofibers treated with 7.7 M HNO_3 at 110°C exhibited the highest capacitance.*

Keywords: Ordered mesoporous carbon, functionalisation, capacitance, supercapacitors, EDLC

1. INTRODUCTION

Supercapacitors have been studied for use in energy storage applications for electric vehicles and any device requiring a high-pulse discharge profile [1-5]. Based on the principle of energy storage, supercapacitors can be classified into two groups, electric double-layer capacitors (EDLC) and pseudocapacitors [6]. EDLCs store electric charge in the double layer formed at the electrode/electrolyte interface, while pseudocapacitors utilize battery-like redox reactions to store energy.

In recent years, research on the development of mesoporous carbonaceous materials [7-12] for use as supercapacitors has intensified. For example, Jurewicz *et al*. prepared mesoporous carbon from different silica arrays (MCM-48 and SBA-15) via the molding method using propylene or sucrose as the carbon source. Their capacitance was tested in acid, alkaline and organic solutions, and the presence of interconnected mesopores, and secondary micropores was found to increase the active surface area available for the electric double layer over that in a strictly microporous material [13].

*To whom correspondence should be addressed:
Email: ben_portales_mtz@hotmail.com
Phone: +5255 57296000 ext. 68311

Liu *et al*. obtained mesoporous carbon using a resol phenol-formaldehyde resin as a carbon source and MCM-48 (mesoporous silica with pore connections and cubic pore geometry) as a template. The obtained capacitances oscillated between 250 and 150 mF; the materials were compared with microporous coal obtained from the same source, indicating that the mesoporous carbon tends to form a higher double-layer capacitance [14].

Fuertes *et al*. prepared mesoporous carbon using SBA-16 as a template synthesized at 100 and 150°C with polyfurfuryl alcohol as the carbon source and obtained average pore sizes of 3 and 8 nm. Electrochemical measurements on the two types of mesoporous carbons used as capacitor electrodes proved that smaller carbon pores provide better capacitor performance [15].

Xing *et al*. obtained three different types of carbon, two from mesoporous MCM-48 and SBA-15 with sucrose as the carbon source and one from SBA-15 with a Si/Al ratio of approximately 40 and polyfurfuryl alcohol as the carbon source. They found that ordered mesoporous carbons (OMCs) exhibit superior capacitive behavior, power output characteristics and high-frequency performance as evidenced by cyclic voltammetry studies and frequency response analysis. The cyclic voltammograms show superior capa-

citive behaviors for OMCs derived from SBA-15 due to their larger pore size and their 2-D pore symmetry. They conclude that the ordered mesoporous carbons (OMCs) offer great potential as EDLCs, particularly in applications requiring high power output and good high-frequency capacitive performance [16].

Chmiola *et al*. studied carbide-derived charcoal materials with pores averaging 0.6 to 2.25 nm and found that pores smaller than solvated electrolyte ions contribute to the charge storage of a capacitor [17].

Li *et al.* prepared mesoporous carbon from SBA-15 and phenol formaldehyde resin. These materials were functionalized with nitric acid via reflux over various intervals. The carbon materials treated for 1.5 h showed the highest high-rate capacity. They also found that functional groups produced pseudocapacitance, which resulted in an increase in specific capacitance. A specific capacitance of 250 Fg^{-1} was obtained at a scan rate of 1 mVs^{-1} [18]. The synthesized mesoporous carbon was impregnated with ruthenium oxide in a proportion of 10 to 30 wt%, resulting in an increase in the capacitance derived from the contribution of the pseudocapacitance of ruthenium oxide on the surface of the mesoporous carbon [19].

Reports are available regarding the benefits of microwave radiation for reducing reaction times in a variety of polar media due to the interactions of the molecules with an electromagnetic field generating effective collisions and, therefore, homogeneity and rapid heating to reach the activation energy [20].

In this paper, the capacitance of carbon fibers synthesized via the molding method using SBA-15 with sucrose as a carbon source is presented. The obtained carbon fibers were functionalized with varying solutions of HNO_3 assisted by microwave radiation for 3 minutes at two different temperatures to control the amount and type of functional groups on the surface of the materials. The structure and high surface area were maintained to determine which functional group was a greater contributor to the capacitance.

2. EXPERIMENTAL

2.1. Mesoporous carbon synthesis and surface modification

Mesoporous material, SBA-15, was prepared as described by Zao *et al*. [21] to obtain large-surface-area silica. In a typical synthesis, we dissolved 4 g of triblock copolymer P-123 (BASF Co.) in a 1.5 M solution of HCl (Fermont, 36.5% by vol.) over two hours at 45°C. Then, a silica source (tetraethyl orthosilicate, TEOS, Aldrich, reagent grade) was added dropwise, and the mixture was stirred at constant temperature for 24 h. The obtained solid was aged at 90°C for one day. Finally, the solid was filtered, washed and dried. The template was removed via calcinations at 550°C.

To obtain the mesoporous carbon, we use the method reported by Ryoo *et al*. [22] in which 1 g SBA-15 was impregnated twice with a slightly acidic aqueous solution of sucrose as a carbon source. Then, the mixture was pyrolized for 1 hour at 1000°C. The template (SBA-15) was removed with a 10-wt% HF solution. Surface modifications of the ordered mesoporous carbon were performed in varying concentrations of HNO_3 (1.9, 3.9, 7.7, and 15.5 M) assisted by microwave radiation over 3 minutes at 110 and 120°C. The final product was defined as FCF_xN_y in which x indicates the volume percentage of HNO_3 in the aqueous solution, and y represents temperature.

2.2. Characterisation of the materials

Nitrogen adsorption-desorption isotherms were measured at 77 K using a Micromeritics ASAP 2405. The total surface area and pore volume were determined using the BET (Brunauer-Emmett-Teller) equation and the single point method, respectively. Pore size distribution (PSD) curves were calculated via the BJH (Barrett-Joyner-Halenda) method. The maximum of the PSD curve was used as the average pore diameter. XRD patterns at small angles ($0.5 \leq 2\theta \leq 5°$) were recorded using a Bruker AXS D8 Advance diffractometer with a θ-θ configuration and Cu K_α radiation.

The transmission electron microscopy (TEM) images of the materials were obtained using an FEI Tecnai G^2 30 transmission electron microscope operating at 300 keV. Dry samples were prepared on a lacey carbon grid.

X-ray photoelectron spectra (XPS) were recorded with a Kratos His spectrometer equipped with a dual anode (Mg/Al) and a monochromatic Al source, a 127-mm hemispherical analyzer with a detection system containing 5 channeltrons, and a magnetic immersion lens used to provide high sensitivity and charge compensation. The smallest spot size recorded was 30 μm.

2.3. Electrochemical measurements

All electrochemical measurements were performed at 25°C in a single, conventional, three-electrode test electrochemical cell. The electrolyte used in this study was a 0.5 M aqueous solution of H_2SO_4 (Merck) prepared using distilled water and constantly purged with argon gas (99.999%, chromatographic grade). A platinum mesh was used as the counter electrode and Hg/Hg_2SO_4/0.5 M H_2SO_4 (MSE=0.680 V/NHE) as the reference electrode. The experiments were performed in a VersaSTAT 3 (METEK-PAR) potentiostat and a Pine MSRX rotation speed controller. Prior to obtaining the electrochemical measurements, the solution was degassed with argon for 10 min. The potentials reported herein are relative to a standard hydrogen electrode (NHE). Prior to obtaining the capacitance measurements, cyclic voltammetry (CV) was performed from 0.0 to 1.2 V at 100 mV s^{-1} in an argon-saturated electrolyte to clean the electrode surface and eliminate impurities and oxides. Ten cycles were required to stabilize the current-potential signal. The current density was calculated using the geometric surface area [23].

An ink-type electrode was employed as a working electrode. For the electrochemical experiments, 8 μl of a sonicated mixture of 1 mg catalyst, 32 μl ethyl alcohol (spectrum grade), and 4 μl of a 5-wt% Nafion® solution (Du Pont, 1000EW) were deposited onto a glassy carbon electrode (GC) with a cross-sectional area of 0.19 cm^2.

3. RESULTS AND DISCUSSION

3.1. Structural analysis

Figure 1 shows a comparison of the X-ray diffraction pattern for the carbon fibers obtained via a molding method against those created with an SBA-15 template in which a peak is observed as follows: $0.86° \leq 2\theta \leq 1.02°$. The peak corresponds to a periodic arrangement of fibers in agreement with that of SBA-15 ($2\theta = 0.99°$) for the template mesopores from which the fibers originate, indicating a reverse replica of SBA-15.

The broader and less defined 2θ peak of the carbon fibers found between 0.86 and 1.02° is due to a larger number of distances for

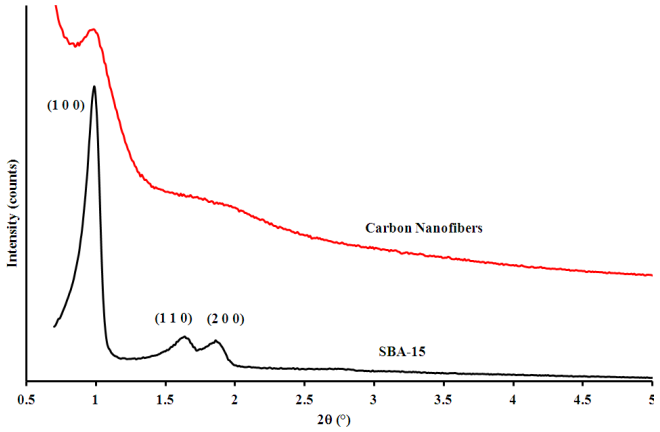

Figure 1. X-Ray diffraction patterns for mesoporous silica and carbon materials

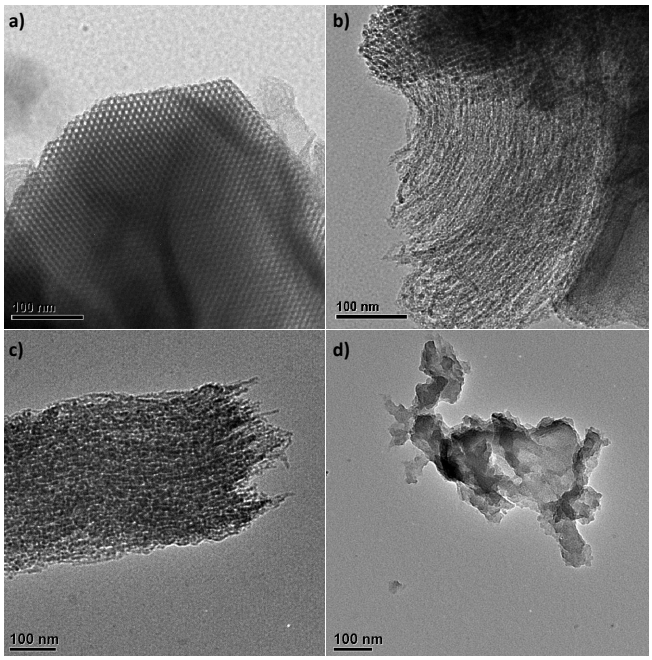

Figure 2. a) Image of a bright field of an SBA-15 particle with a 2-D hexagonal arrangement of the pores. b) Group of fibers arranged in bundles. c) Fibers treated with 7.9 M HCl and 110°C. d) Fibers treated with 18.8 M HCl and 120°C

the plane (1 0 0) of the SBA-15 from which they originate. These distances increase or decrease because the fibers are connected by microfibers formed from the microporous connector belonging to the main pores on the SBA-15. Some of these microfibers could collapse during the treatment or silica removal, so the nanofibers are less fixed and can move away from one another, which is reflected in the variation in the distances that yield a broader (1 0 0) reflection. In contrast, the disappearance of secondary peaks can be attributed to the deformation of the hexagonal array.

Figure 2(a) shows the hexagonal pore arrangement of SBA-15

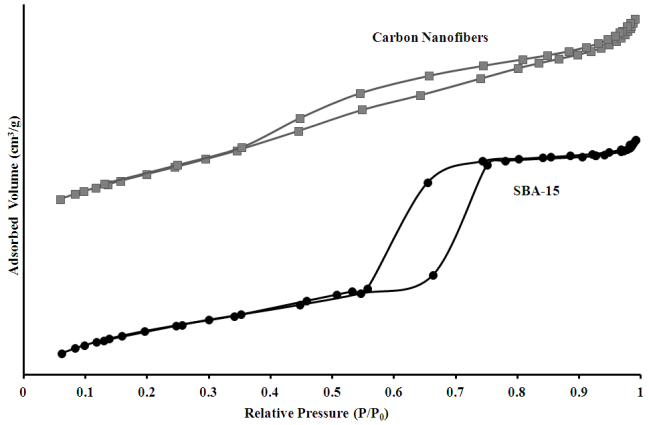

Figure 3. Comparison of the adsorption-desorption isotherms of nitrogen on the carbon fibers and SBA-15

and confirms the XRD results (Figure 1) demonstrating that these pores are parallel to one another with small interconnections between them that derive from the interlocking chains of the copolymer used as the template.

From this Figure, one can observe that the fibers follow the same direction (Figure 2(b)), demonstrating that they come from the parallel channels of SBA-15 but are more flexible because they are made only of carbon and can bend without breaking. In contrast, Figure 2(b) shows a fibre beam; this formation suggests that the fibers are joined by microconnectors originating from the micropores in the SBA-15. Similarly, at the end of the beam, bent fibers are randomly arranged, also suggesting the existence of the fibers as individual entities. Although the image shown in Figure 2(b) reveals a relatively high order, the morphology of the bulk material is varied, as shown by the XRD (1 0 0) peak broadening.

Finally, in Figure 2(c) and 2(d), the morphology of the as-treated 7.9 and 15.8 M samples is shown at 110 and 120°C, respectively. The former maintains the structure of the replicas, and the latter, having undergone more severe treatment with heat and acidity, has lost its ordered structure.

3.2. Textural properties analysis

Figure 3 shows the adsorption-desorption isotherm of nitrogen for the SBA-15 material appearing as a type IV isotherm (according IUPAC), which is characteristic of mesoporous materials [24]. This isotherm shows a significant increase in the amount of nitrogen adsorbed at intermediate relative pressures (0.55 to 0.75). The nitrogen adsorption occurs through a multilayer-filling mechanism and contains an H1-type hysteresis that is characteristic of materials with particles crossed by nearly cylindrical channels or made by aggregates or agglomerates of spheroidal particles with pores of uniform shape and size [24]. This material had a surface area of 850 m^2/g.

The carbon fibers have an isotherm that resembles the type II isotherm (IUPAC), as shown in Figure 3; however, the isotherm of the carbon fibers has a softer slope and no inflections. A type H3 (IUPAC) hysteresis is observed and is characteristic of solids consisting of aggregates or clusters of particles formed by parallel plates [24].

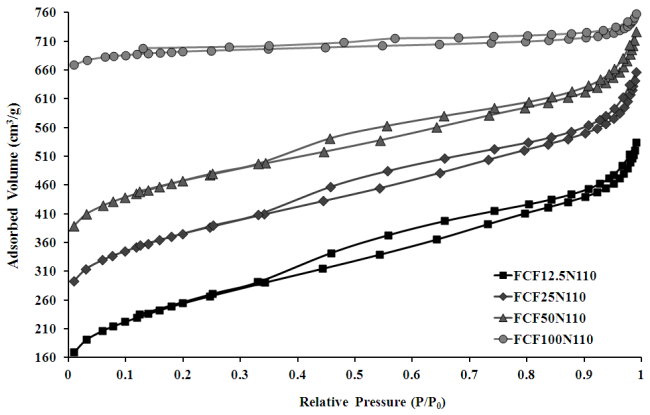

Figure 4. Adsorption-desorption isotherms of carbon fibers functionalized at 110°C

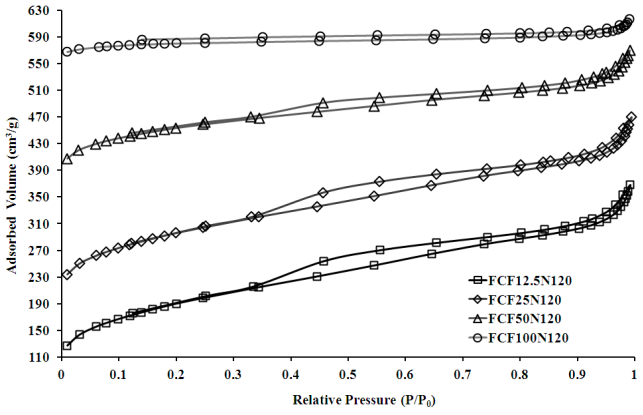

Figure 5. Adsorption-desorption isotherms of carbon fibers functionalized at 120°C

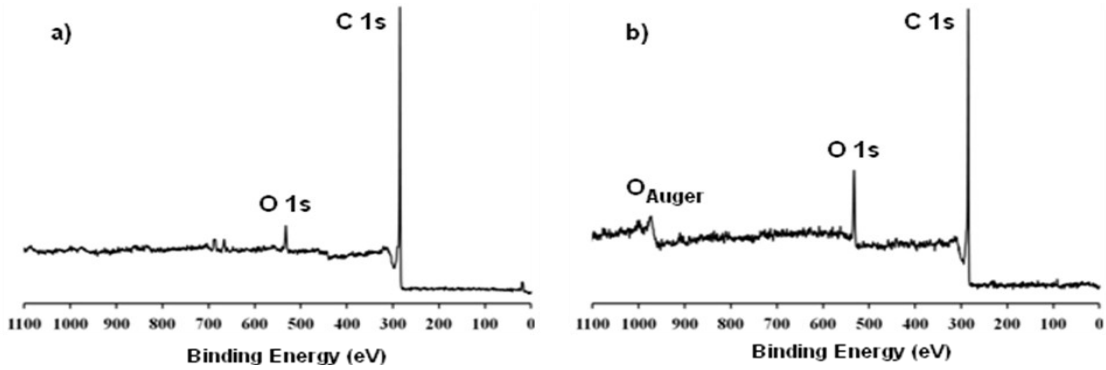

Figure 6. High-resolution XPS spectra of a) FCF0N and b) FCF50N110 showing the principal peaks

In Figure 4 (fibers treated at 110°C) and Figure 5 (fibers treated at 120°C), the carbon fibers present a type of isotherm that resembles a type II isotherm (IUPAC) [24]; however, the isotherm of the carbon fibers has a soft slope and less pronounced inflections in the ranges of $0.16<P/P_0<0.33$ and $0.4<P/P_0<0.71$, which are characteristic of the type IV isotherms typical of mesoporous materials. The presence of these inflections is consistent with the molding method used with SBA-15 (a mesoporous material).

A type H3 (IUPAC) is observed [24], which is characteristic of solids consisting of aggregates or clusters of particles formed by parallel plates. As shown in Figures 4 and 5, the arrangement of the pores in the fibers follows a linear path, which forms a layer composed of fibers.

Initially, material exhibits monolayer adsorption. Following the monolayer adsorption, condensation of the liquid occurs in which the intragranular spaces are filled due to the amorphous nature of the material. The various isotherms differ substantially in their slopes, which are dependent on the amount of nitrogen adsorbed that is directly translated into the surface of the material. The materials treated at 110°C with low concentrations of HNO_3 have lower slopes than either those treated with concentrated HNO_3 or those treated at 120°C.

In Table 2, a summary of textural properties is presented in which it is noted that all the samples are within the range of mesoporous materials and present features that could be beneficial to support electrocatalysts [24]. The average pore size oscillates between 2 and 4 nm independent of the treatment conditions, but a diminution in the surface area in the overall TEM images indicates a degradation in the microfibre joint between the main fibers, causing a channel collapse and a loss of order. Therefore, the average pore size could not be indicative of the electrochemical activity. Instead, the surface area provides a better correlation between the structure and the electrochemical activity, as shown by the electrochemical results.

3.3. Chemistry surface analysis

Through an X-ray photoelectron spectroscopy (XPS) analysis, the population of functional groups on the fibre surfaces was obtained. Figure 6 presents an example of the XPS spectra obtained: a) sample without treatment and b) sample treated with a 50/50 aqueous solution of HNO_3 at 110°C. Four different primary types of peaks were observed. The first peak, with a binding energy between 280 eV and 300 eV, corresponds to C 1s; the second, with a binding energy between 525 eV and 540 eV, corresponds to O 1s; and the final two peaks, with binding energies of approximately 975 eV and 1000 eV, both derive from the emission of oxygen's Auger electrons [25-32].

Deconvolution of the C 1s region (Figure 7) in the XPS spectra

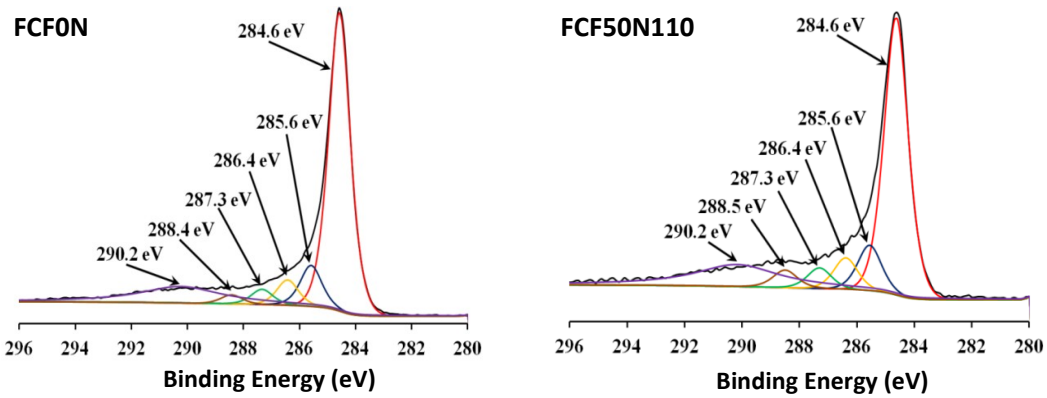

Figure 7. High-resolution XPS C 1s spectra of carbon nanofibers FCF0N and FCF50N110 and the assignment of the binding energy in eV for the C 1s region

of samples FCF0N and FCF50N110 (Figure 6) shows six peaks that represent carbon-carbon bonding (284.6 eV); the secondary chemical shift, which is the effect of the carboxyl group on the unsubstituted carbon atom in the C-COO- structure (285.3–285.6 eV); carbon present in phenolic, alcohol, ether or C=N groups (286.4–286.7 eV); carbonyl or quinone groups (287.2–287.5 eV); carboxyl or ester groups (288.4–289 eV); and the interaction of ejected core electrons with plasmons from the conduction in the carbon materials (290.0–290.4 eV) [25-32]. All the functional groups of the carbon species are present in all of the samples, and these groups evolve as the molarity of the acid used increases.

The peak corresponding to the carboxylic group (288.4–289.3 eV) in FCF50N110 exhibits greater intensity, as this material was treated with a highly concentrated solution (7.7 M) of HNO_3. In addition, the intensity of this peak slightly increases with increasing molarity of the acid used. The other peaks exhibit no noTable change due to minor relative increases in the functional groups on the surface.

The calculated percentages of the carbon atoms and their functional groups are shown in Table 1. The percentages are relative and adjusted only to carbon. A decreased concentration of the C-C species can be observed in the samples treated at 110°C. Although the low concentrations (1.9–3.9 M) in the amount of C-C remain consistent, changes can be observed in the oxygenated functional groups; however, the surface area of these materials is constant.

At medium and high concentrations (7.7–15.5 M), there is a more marked decline in the C-C species and an increase in the oxygenated functional groups, especially in the population of the carboxyl groups. This functional group exhibits a similar increase with concentrations of 1.9 and 3.8 M HNO_3 independent of the temperature. At concentrations of 7.7 and 15.5 M, the population of carboxyl groups doubles compared with the materials treated with more dilute acid. In summary, higher acid concentrations and higher temperatures increase the number of carboxyl groups but decrease the surface area.

For materials treated at 120°C, a decrease in the C-C species is more easily observed through an increase in the oxygenated functional groups. In contrast, the materials treated at 110°C exhibited larger surface areas than those treated at 120°C. The relative percentage of carboxyl groups was the highest in the sample treated with a 15.5-M solution of HNO_3 at 120°C.

3.4. Electrochemical Analysis

Figure 8 shows the voltammograms of the FCF0N and FCF50N110 samples; the latter exhibits a higher current density, indicating a lower resistance of the material. Both samples show two symmetric peaks, which indicate a reversible process on the surface of the sample due to the functional groups present. This fact is confirmed by the observation that the FCF50N110 sample exhib-

Table 1. Relative atomic percentage of functional groups (carbon atoms) on the surface

Sample	C-C [%]	C-COO- [%]	C-O- [%]	C=O [%]	COO- [%]
FCF-0N	80.78	8.65	5.41	3.21	1.95
FCF-12.5N110	76.41	10.21	6.30	4.17	2.91
FCF-25N110	76.58	8.15	7.06	4.74	3.47
FCF-50N110	75.7	9.22	6.40	4.72	3.96
FCF-100N110	64.88	12.75	8.34	4.40	9.63
FCF-12.5N120	76.14	11.01	5.56	4.11	3.18
FCF-25N120	75.00	10.94	5.81	4.62	3.63
FCF-50N120	71.89	11.49	5.47	4.53	6.63
FCF-100N120	64.79	11.73	4.66	4.99	13.83

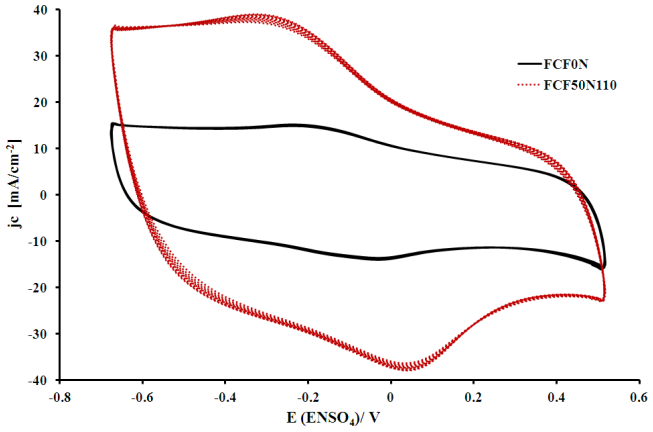

Figure 8. Cyclic voltammograms for FCF0N and FCF50N110 at a scan rate of 5 mV s^{-1}

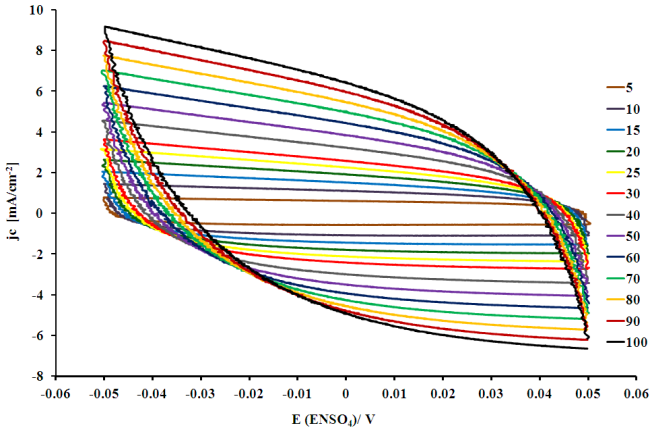

Figure 9. Cyclic voltammograms for FCF0N at varying scan rates from 5 to 100 mV s^{-1}

its a greater definition in its peaks compared with the FCF0N sample, and the latter contains fewer functional groups. The samples exhibited high stability; the peak shape does not change, and there was no significant decrease in the current density.

Table 2 collates the results of the textural properties, the surface chemistry and the capacitances for the samples studied. The second column presents the molarity of the acid used to functionalise materials, the third column presents the results of the capacitance measurement, the next three columns provide the values of the textural properties, and finally, the last two columns present the relative atomic percentages of carbon and oxygen on the surface of the nanofibers.

Table 2 indicates that the samples treated at 110°C exhibit a higher capacitance than those treated at 120°C. The samples functionalized with low concentration solutions (1.9 and 3.9 M HNO_3) exhibited similar capacitances and, likewise, had the largest surface areas (approximately 900 m^2/g). With a similar pore volume (0.78 cm^3/g) and pore diameter (3.5 nm), the sample treated with the 7.7-M solution at 110°C had the highest capacitance, which was approximately 50% higher than the samples treated with dilute solutions, with a similar pore diameter and pore volume; however, its surface area was 3.34% lower than the samples treated with dilute solutions. This observation can be explained by the presence of a larger number of carboxyl groups on the surface.

Although the samples treated with a 15.5-M solution of HNO_3 had the highest number of functional groups, these samples had the lowest capacitance, possibly due to their low surface area, which was 53% lower than the samples treated with the lower-concentration solutions. In the samples treated at higher temperatures, the surface area decreased six-fold. Because samples with higher capacitances have very similar surface areas, pore volume and pore diameters, differences in the capacitance can be attributed to the amount and type of surface functional groups.

Figure 9 shows the voltammograms of the FCF0N sample measured at different scan rates, and Figure 10 shows the voltammograms of the sample treated at 110°C with a 50%-by-volume solution of HNO_3. In both Figures, the voltammograms become tilted with an increase in the potential-sweep rate. Results obtained indicates that at high sweep rates, the ohmic resistance for the electrolyte motion in the carbon pores affects the double-layer formation mechanism in which the stored charge is recognized for distribution. The increase in the induced current with the sweep rate would have intensified the potential difference between the top and bottom of the pores, thus resulting in a delayed current response, as shown in the tilted voltammograms.

The findings of these authors indicate that higher capacitances

Table 2. Textural properties and capacitance of the chemically functionalized carbons

Sample	Molarity HNO_3	Capacitance mF/cm^2	S_{BET} m^2/g	V_{tot} cm^3/g	D_{prom} nm	O [%]	C [%]
FCF0N	0	88	824	0.79	3.8	4.96	95.04
FCF12.5N110	1.9	90	903	0.78	3.5	9.69	90.31
FCF25N110	3.9	101	904	0.78	3.5	10.85	89.15
FCF50N110	7.7	159	873	0.74	3.4	11.67	88.33
FCF100N110	15.5	11	424	0.22	2.1	21.58	78.42
FCF12.5N120	1.9	80	673	0.54	3.2	10.33	89.67
FCF25N120	3.9	67	692	0.54	3.1	12.01	87.99
FCF50N120	7.7	50	537	0.4	3.0	15.34	84.66
FCF100N120	15.5	5	108	0.09	3.3	24.4	75.6

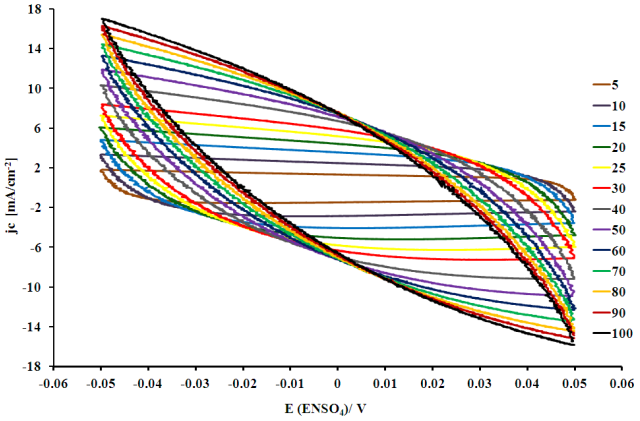

Figure 10. Cyclic voltammograms for FCF50N110 at varying scan rates from 5 to 100 mV s^{-1}

can be expected in materials with greater surface areas and more functional groups on their surfaces, which can be achieved by obtaining a more highly ordered material and by searching for different synthesis methods.

4. CONCLUSIONS

Ordered mesoporous carbon fibers were synthesized from SBA-15 using a molding method with sucrose as a carbon source, and further functionalisation was performed with HNO_3 assisted by microwave radiation at 110°C and 120°C for 3 min. These techniques were shown to be a good method for creating functional groups as a function of the HNO_3 concentration and the temperature. At higher temperatures and greater HNO_3 concentrations, the number of carboxyl groups increases, but the surface area decreases. Better capacitances were obtained for the samples created with a compromise between surface area and functional groups. The samples treated with 7.7 M HNO_3 at 110°C exhibited the highest capacitance among the samples measured. Finally, by altering the sweep rates, one can observe a change in the ohmic resistance for the electrolyte motion into the carbon fibers, leading to a stable double-layer formation at lower scan rates.

5. ACKNOWLEDGMENTS

The support of CONACYT and IPN-SIP through projects CB-157925 SIP MULTI-1338, SIP 20120475 and SIP 20120445 is gratefully acknowledged.

REFERENCES

[1] G. Gryglewicz, J. Machnikowski, E. Lorenc-Grabowska, G. Lota, E. Frackowiak, Electrochim. Acta, 50, 1197 (2005).
[2] X. Dong, W. Shen, J. Gu, L. Xiong, Y. Zhu, H. Li, and J. Shi, J. Phys. Chem. B, 110, 6015 (2006).
[3] Y. Lei, C. Fournier, J.-L. Pascal, F. Favier, Micropor. and Mesopor. Mater., 110, 167 (2008).
[4] D.-W. Wang, F. Li, Z.-G. Chen, G. Q. Lu, and H.-M. Cheng., Chem. Mater., 20, 7195 (2008).
[5] H. Pan, J. Y. P. Feng, Nanoscale Res. Lett., 5, 654 (2010).
[6] B.E. Conway, "Electrochemical Supercapacitors, Scientific Fundamentals and Technological Applications", Kluwer Academic, New York, 1999.
[7] H. Li, H. Xi, S. Zhu, Z. Wen, R. Wang, Micropor. Mesopor. Mater., 96 357 (2006).
[8] A. Guha, W. Lu, T.A. Zawodzinski, D.A. Schiraldi, Carbon, 45, 1506 (2007).
[9] A.-H. Lu, W. Li, Z. Hou, F. Schüth, Chem. Commun.,10, 1038 (2007).
[10]M.J. Lázaro, L. Calvillo, E.G. Bordejé, R. Moliner, R. Juan, C.R. Ruiz, Micropor. Mesopor. Mater., 103, 158 (2007).
[11]P.A. Bazuła, A.-H. Lu, J.-J. Nitz, F. Schüth, Micropor. Mesopor. Mater., 108, 266 (2008)
[12]M. Jaroniec, J. Gorka, J. Choma, A. Zawislak, Carbon, 47, 3034 (2009).
[13]K. Jurewicz, C. Vix-Guterl, E. Frackowiak, S. Saadallah, M. Reda, J. Parmentier, J. Patarin, F. Béguin, J. of Phys. and Chem. of Solids, 65, 287 (2004).
[14]H.Y. Liu, K.-P. Wang, H. Teng, Carbon, 43, 559 (2005).
[15]A.B. Fuertes, G. Lotaa, T.A. Centeno, E. Frackowiak. Electrochim. Acta, 50, 2799 (2005).
[16]W. Xing, S.Z. Qiao, R.G. Ding, F. Li, G.Q. Lu, Z.F. Yan, H.M. Cheng, Carbon, 44, 216 (2006).
[17]J. Chmiola, G. Yushin, Y. Gogotsi, C. Portet, P. Simon, P.L. Taberna, Science, 313, 1760 (2006).
[18]H. Li, H. Xi, S. Zhu, Z. Wen, R. Wang, Micropor. and Mesopor. Mater., 96, 357 (2006).
[19]H. Li, R. Wang, R. Cao, Micropor. and Mesopor. Mater., 111, 32 (2008).
[20]E. Juaristi, "Aplicaciones de microondas en química y en biología", El Colegio Nacional, México, 2009.
[21]D. Zhao, J. Sun, Q. Li, G.D. Stucky, Chem. Mater., 12, 275 (2000).
[22]S. Jun, S.H. Joo, R. Ryoo, M. Kruk, M. Jaroniec, Z. Liu, J. Am. Chem. Soc., 122, 10712 (2000).
[23]R. González Cruz, O. Solorza Feria. J. Solid State Electrochem., 7, 289 (2003).
[24]G. Leofanti, M. Padovan, G. Tozzola, B. Venturelli, Catal. Today, 41, 207 (1998).
[25]S.M. Lee, "Handbook of Composite Reinforcements", Palo Alto CA: VCH Publishers Inc 1993.
[26]W.H. Lee, W.H. Kim, W.J. Lee, J.G. Lee, R.C. Haddon, P.J. Reucroftd, Appl. Surf., 181, 121 (2001).
[27]D. Briggs, G. Beamson, Anal. Chem., 64, 1729 (1992).
[28]H. Ago, T. Kugler, F. Cacialli, W.R. Salaneck, S.P. Shaffer, A.H. Windle, J. Phys. Chem. B, 103, 8116 (1999).
[29]G. Nansé, E. Papirer, P. Fioux, F. Moguet, A. Tressaud, Carbon, 35, 175 (1997).
[30]A. Proctor, P. Sherwood, Anal. Chem. 54, 13 (1982).
[31]S. Jackson, R. Nuzzo, Appl. Surf. Sci., 90, 195 (1995).
[32]J. F.Watts, J.Wolstenholme, "An Introduction to Surface Analysis b XPS and AES", West Sussex Englan: John Wiley & Sons Ltd 2003.